Ultrasonics Sonochemistry 19 (2012) 830–840

Contents lists available at SciVerse ScienceDirect

Ultrasonics Sonochemistry

journal homepage: www.elsevier.com/locate/ultsonch

Synthesis of manganese oxide nanocrystal by ultrasonic bath: Effect of external magnetic field

Tahereh Rohani Bastami, Mohammad H. Entezari *

Department of Chemistry, Ferdowsi University of Mashhad, 91775 Mashhad, Iran

ARTICLE INFO

Article history:
Received 5 October 2011
Received in revised form 23 November 2011
Accepted 28 November 2011
Available online 13 December 2011

Keywords:
Hausmannite
Manganite
External magnetic field
Superparamagnetic
Ferrimagnetic

ABSTRACT

A novel technique was used for the synthesis of manganese oxide nanocrystal by applying an external magnetic field (EMF) on the precursor solution before sonication with ultrasonic bath. The results were compared in the presence and absence of EMF. Manganese acetate solution as precursor was circulated by a pump at constant speed (7 rpm, equal to flow rate of 51.5 mL/min) in an EMF with intensity of 0.38 T in two exposure times (t_{MF}, 2 h and 24 h). Then, the magnetized solution was irradiated indirectly by ultrasonic bath in basic and neutral media. One experiment was designed for the effect of oxygen atmosphere in the case of magnetic treated solution in neutral medium. The as prepared samples were characterized with X-ray diffraction (XRD), Fourier transform infrared (FTIR) spectroscopy, transmission electron microscopy (HRTEM, TEM), energy-dispersive spectrum (EDS), and superconducting quantum interference device (SQUID) analysis. In neutral medium, the sonication of magnetized solution (t_{MF}, 24 h) led mainly to a mixture of Mn_3O_4 (hausmannite) and γ-MnOOH (manganite) and sonication of unmagnetized solution led to a pure Mn_3O_4. In point of particle size, the larger and smaller size of nanoparticles was obtained with and without magnetic treatment, respectively. In addition, the EMF was retarded the nucleation process, accelerated the growth of the crystal, and increased the amount of rod-like structure especially in oxygen atmosphere. In basic medium, a difference was observed on the composition of the products between magnetic treated and untreated solution. For these samples, the magnetic measurements as a function of temperature were exhibited a reduction in ferrimagnetic temperature to T_c = 39 K, and 40 K with and without magnetic treatment, respectively. The ferrimagnetic temperature was reported for the bulk at T_c = 43 K. A superparamagnetic behavior was observed at room temperature without any saturation magnetization and hysteresis in the measured field strength. The effect of EMF on the sample prepared in the basic medium was negligible but, in the case of neutral medium, the EMF affected the slope of the magnetization curves. The magnetization at room temperature was higher for the samples obtained in neutral medium without magnetic treatment. In addition, a horizontal shift loop was observed in neutral medium at low temperature.

1. Introduction

Numerous papers focused on the effect of magnetic field on the crystallization and precipitation of organic and inorganic compounds [1–5]. Freitas et al. [1] studied the influence of magnetic field on the crystallization of the zinc sulfate-water and copper sulfate-water. Nývlt and Kricková [2], found that the magnetic field increased the nucleation kinetics during crystallization of $MgSO_4$ from aqueous solutions. Higashitani et al. [3], studied the influence of magnetic exposure on the formation of $CaCO_3$ crystals. They used a magnetic flux density less than 0.3 T with an exposure time more than 10 min. Under these conditions, the nucleation of $CaCO_3$ was suppressed but the growth of crystals was accelerated [3]. In addition, the magnetic exposure accelerated the formation of aragonite crystals [3]. Madsen [4] investigated the magnetic field on the precipitation of paramagnetic and diamagnetic inorganic salts. It was concluded that only phosphates and carbonates with diamagnetic metal ion are affected, through enhancement of nucleation and growth rates. Mitrovic [5] studied the effect of magnetic field on the crystallization of $MnCl_2{\cdot}4H_2O$.

Recently a new attention has been paid to the synthesis of nanomaterials especially transition-metal oxides which are due to its extensive applications [6]. Up to now, it has been proposed several synthesis approaches for the preparation of nanomaterial [7–10]. However, based on the best of our knowledge, there is no report about the fabrication of nanostructure material using magnetic field exposure on the precursor solution.

Manganese oxide and oxohydroxide nanostructures have attracted considerable attention because of their potential applications in many fields including separation, chemical sensing devices, biology and electronics [11,12]. There are many works about the synthesis of manganese oxide with classical and solvothermal methods [13,14]. These approaches require long reaction

* Corresponding author.
E-mail address: moh_entezari@yahoo.com (M.H. Entezari).

1350-4177/$ - see front matter © 2011 Elsevier B.V. All rights reserved.
doi:10.1016/j.ultsonch.2011.11.019

time such as 12–72 h at different temperatures and pressures. Another method used for the preparation of manganese oxide is sol–gel [15]. The sol–gel method has some disadvantageous like expensive, time consuming, and polluting. The conventional high-temperature calcinations of the products lead to inconsistency in product quality and it is an uneconomical procedure [16].

Currently, there is a trend toward simple, low temperature solution method for the preparation of nanoparticle. One of the novel and simple method for the synthesis of nanomaterial is sonochemistry [17,18]. Sonochemistry as a unique and powerful technique is used for the synthesis of different compounds in the normal condition. Synthesis of material via ultrasonic irradiation led to high activity in catalysis due to their particles size and high surface area [19]. The chemical and physical effects of ultrasonic irradiation originate from acoustic cavitations, which is, the formation, growth and implosive collapse of bubbles in a liquid [20]. The implosive collapse of the bubbles produces a localized hotspot via adiabatic compression or shock wave formation within the gas phase of the collapsing bubble. This harsh condition generates transient temperatures of ~5000 K, pressure of 1800 atm and cooling rates in excess of 10^{10} K/s which determined from hotspots theory [20]. Most of the works for the synthesis of nanomaterials by ultrasonic waves were focused on the preparation of nanomaterials by using high intensity ultrasonic probe [21–23].

There are some works in the literature about the synthesis of Mn_3O_4 with ultrasonic irradiation using high intensity ultrasonic probes [24–26]. Recently, we have reported for the first time the synthesis of Mn_3O_4 nanoparticles in different basic media by ultrasonic bath as a low power ultrasonic irradiation source [27].

Regarding to the morphology and shape of nanomaterials, most of the works focused on the synthesis of 3D nanoparticles. In the past few years, a great attention has been paid to the synthesis of 1D nanomaterials for their unique properties in electronics, photonics, sensing device, etc. [28,29]. This structure was synthesized by vapor deposition [30], solvothermal reaction [31], and surfactant-assisted method [32]. Ultrasonic irradiation could offer an attractive method for the preparation of 1D nanomaterial [33,34]. Due to more efficient mixing [35] and faster mass transfer of the reactant under action of microjet and shock wave of cavitation process [36], ultrasonic irradiation can significantly improve crystal nucleation and growth. It was suggested that the ultrasonic wave probably has the ability to improve oriented-attachment of primary nanoparticles and lead to 1D nanoparticle [34].

This study focuses on the synthesis of manganese oxide nanoparticles using bath ultrasonic irradiation in neutral and basic media. In the absence of ultrasonic irradiation, no product was obtained in neutral medium. The precursor solutions were exposed to EMF (0.38 T) and then sonicated. As our best knowledge, there is no report about the sono-synthesis of nanomaterial using a treated solution with EMF and also this is the first report about the synthesis of nanorod structure at low temperature and normal condition without any further post treatment.

2. Experimental

2.1. Material

Manganese(II) acetate, $4H_2O$, and sodium hydroxide were purchased from Merck Company. Milli-Q water was used with a resistivity not less than 18.2 MΩ cm^{-1}.

2.2. Procedure

2.2.1. Preparation of manganese oxide without EMF

Manganese acetate was used as a precursor for the synthesis of manganese oxide nanoparticles. In neutral medium (pH 6.8), 4.6 g of the precursor compound was dissolved in 30 mL milli-Q water. The prepared solution was poured in an erlenmayer as a sonochemical reaction vessel. The erlenmayer was placed at the top of the water in the bath and then sonicated. The optimum horizontally position for the reaction vessel in the bath is important. The vessel should be located at the position with the maximum disturbance on the surface of liquid inside the vessel. The same glass vessel should be used each time as the differences in the thickness of the glass base influence on the ultrasonic power transferred into the reaction system. The amount of transferred energy to the reaction is low and normally it is in the range of 1–5 W cm^{-2} [37]. The synthesis was carried out with Branson 8510E-DTE ultrasonic bath, commonly used for cleaning purposes in laboratories (40 kHz-overall dimensions: 24 in. × 18 in. × 14.5 in.; internal dimensions: 19.5 in. × 11.5 in. × 6 in.). Based on different applied conditions, the total aging time of sonication was 180 min and the temperature was set at 60 ± 2 °C. The reaction products were centrifuged, washed with distilled water and dried at 100 °C. It should be mentioned that the visual induction period (the time requires to change color from colorless) for the appearance of nanoparticles was about 5 min. In the basic medium, the pH of solution was adjusted at 8.0 by adding dropwise (1 drop/min) of sodium hydroxide to control the pH of solution before sonication. All experiments were carried out in ambient condition under air atmosphere. Also, one experiment was run in the absence of ultrasonic irradiation (stirrer method) in neutral medium and the other conditions were the same as experiment under ultrasonic irradiation and neutral medium. In the basic condition, Rohani Bastami and Entezari, compared the stirrer method with ultrasonic irradiation [27].

2.2.2. Preparation of manganese oxide with EMF

In neutral medium, 4.6 g of manganese acetate was dissolved in 30 mL milli-Q water. This solution was circulated in the presence of EMF for 24 h and 2 h by circulating pump (Scheme 1). The EMF was generated by a couple of permanent magnets with intensity of 0.38 T and the solution was circulated through the EMF with flow rate of 51.5 mL/min. The magnetized solution was poured in an erlenemayer as a sonochemical reaction vessel and then placed on the optimum position in the bath and sonicated. The time of sonication, the temperature, and the position of erlenmayer in the bath were the same as sonication without EMF. The visual induction periods in this case were in the range of 25–30 min, and 8–10 min for 24 h and 2 h circulating in the presence of EMF, respectively. The reaction products were centrifuged, washed with distilled water and dried at 100 °C. One experiment was run in the O_2 atmosphere. In this case, the magnetized solution for 24 h was purged with O_2 for 1 h before sonication and the purge of oxygen was continued during the sonication. The visual induction period was about 10 min. Also, one experiment was run under the same conditions with Ar atmosphere in neutral pH with and without EMF.

The induction period for the colloidal dispersion of manganese oxide were monitored by UV–vis absorption spectroscopy. Fig. 1 shows the UV–vis absorption spectrum in the case of manganese oxide in neutral media without EMF. At the beginning (before sonication), the UV–vis spectrum of a freshly prepared solution of manganese acetate in milli-Q water exhibited a wide absorption band with an onset at 400 nm (Fig. 1). After 5 min, this band becomes wider and the onset shifts to about 600 nm which related to the induction period.

In the basic condition, the pH of solution was adjusted at 8.0 by adding of sodium hydroxide dropwise (1 drop/min) in the magnetized solution and the total volume was fixed at 30 mL. The other conditions were the same as neutral medium.

2.3. Characterization and instrument

The size and morphology of the samples were characterized using a JEOL-2010 TEM operating at 200 kV of accelerate voltage.

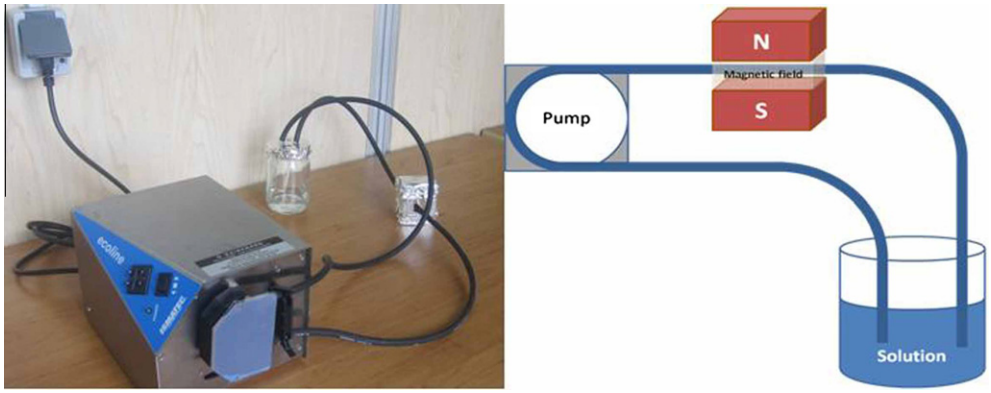

Scheme 1. Experimental setup for circulation of manganese acetate solution in EMF.

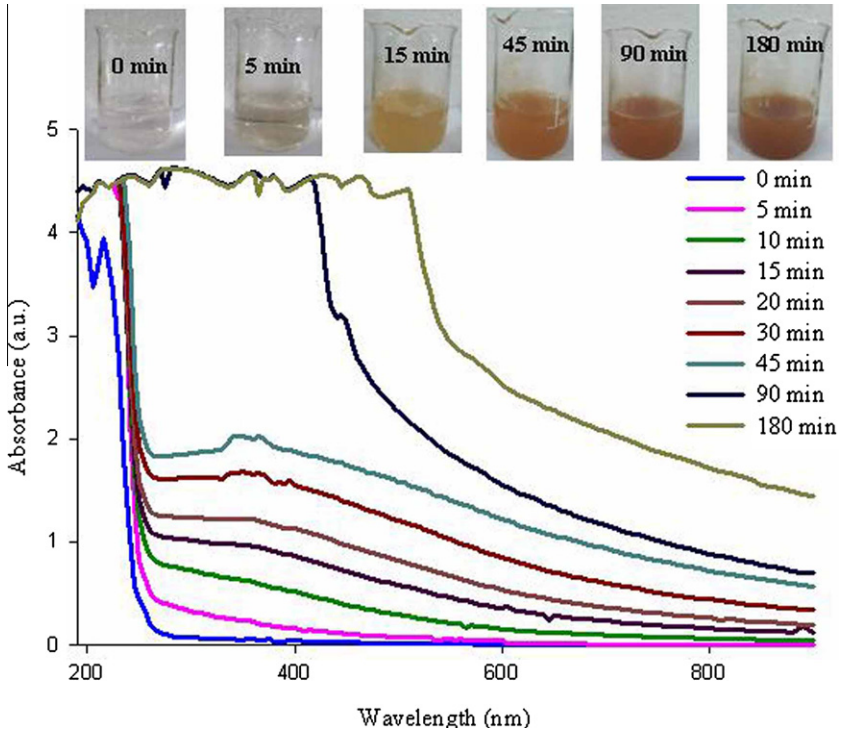

Fig. 1. UV–vis absorption spectra of manganese acetate solution (4.6 g, milli-Q water 30 mL) immediately after preparation (0 min) and during the sonication.

The TEM (LEO 912 ab, ziess Germany, 120 kV) was also used for the characterization of the product. The sample was dispersed in ethanol and dropped on the copper grid before loading to the instrument. The XRD of the products was recorded on Bruker, D8 ADVANCE, Germany (X-ray tube anode: Cu, wavelength: 1.5406 Å (Cu Kα) filter: Ni). The FTIR of the samples were recorded using Nicolet 6700 in the range of 400–4000 cm^{-1} with ATR accessories. The magnetization measurements were carried out using a Magnetic Property Measure System (MPMS, Quantum design) under magnetic fields up to 10,000 Oe at 300 K and 10 K.

A pump by Ecoline VC360 ISM 1076 model was used for circulating the solution through the EMF. The hydrogen peroxide concentration was measured by UV–vis spectrophotometer (Unico 2800).

2.4. Calorimetry

The ultrasonic intensity of bath sonicator at 30 °C was measured through calorimetric method [38] and it was 0.30 W cm^{-2} and the ultrasonic density was 0.011 W cm^{-3}.

2.5. Formation of H_2O_2

Hydrogen peroxide concentration was determined iodometrically [39]. By measuring the concentrations at different times, the rate of formation of H_2O_2 was 0.752 μM min^{-1}at 60 °C.

3. Results and discussion

3.1. XRD analysis

The XRD patterns of the samples under different conditions using low power ultrasonic irradiation (bath sonicator) show the crystalline nature of the products (Supplementary Figs. S1–S3). The products are well crystallized and the XRD peaks of the samples can be indexed to (101), (112), (103), (211), (220), and (224) for the tetragonal hausmannite structure in accordance with JCPDS card of Mn_3O_4 (JCPDS-24-0737) under different conditions. In the absence of EMF, the products are pure and no peaks have been detected for the impurity phases. The XRD pattern of the

samples in the presence of EMF shows a mixture of phases in the product. Table 1 summarizes the composition of the products with different t_{MF}.

In sonication of the magnetized samples under the neutral medium and ambient atmosphere, a small quantity of MnO_2 as an impurity was obtained for t_{MF}, 2 h. But, a longer time of magnetization (t_{MF}, 24 h) led to a mixture of Mn_3O_4 and MnOOH with a few amount of MnO_2 and Mn_2O_3. Table 1 shows the presence of 24.7% manganite (MnOOH) phase in the sample with t_{MF}, 24 h. It indicates that the t_{MF} affects on the production phase. Another point is the lattice parameter (c) for Mn_3O_4 phase which increased by increasing the t_{MF}. When O_2 atmosphere was used in the neutral medium, a mixture of Mn_3O_4 and MnOOH with a few amount of Mn_2O_3 were obtained. According to the XRD peaks, it is proposed that the EMF may be led to the decrease of crystal growth in the (1 0 1), (2 1 1) and (1 0 3) axis and increase of crystal growth in the (2 2 4) axis.

In the basic condition, the impurity phases are MnO_2 and Mn_2O_3. It is not observed any peaks corresponding to the MnOOH phase and the amount of impurities is nearly similar for different t_{MF}. In addition, the crystal growth was not changed significantly in the presence and absence of EMF. In this case, the lattice parameter was also increased with t_{MF}.

3.2. FTIR analysis

The FTIR analysis on the prepared samples was performed (Supplementary Fig. S4). The vibrational spectra of manganese oxides can be divided into three sections in the range of 200–450 cm^{-1}, 450–600 cm^{-1}, and 600–750 cm^{-1}, where stretching, bending, and wagging vibrations of MnO_n units are showing up [40]. Two significant absorption peaks are observed in the range of 450–650 cm^{-1} for all of the samples. The vibration frequency at 602 cm^{-1} is the characteristic of Mn–O stretching modes in tetrahedral sites, whereas the vibration frequency at 494 cm^{-1} corresponds to the distortion vibration of Mn–O in an octahedral environment. The peak in the range of 3380–3410 cm^{-1} could be assigned to νOH vibration of weakly bonded (physisorbed) water molecules. The vibration band at 1100 cm^{-1} is due to δ1-OH and the peak around 1170 cm^{-1} is due to δ2-OH. In O_2 atmosphere, the observed intense band at 2080 cm^{-1} possibly belongs to binary combinations involving OH librations of manganite (γOH + δOH) and the band at 2670 cm^{-1} is fundamental OH stretching related to the hydrogen bonding with an O═H···O length of 2.6 Å which originated from manganite [41–43]. The third vibration band, located at a weaker wave number 417 cm^{-1} can be attributed to the vibration of manganese species (Mn^{3+}) in an octahedral site [16,44]. For the samples obtained in basic medium, strong and broad peaks were observed with maximum at 3410, and 3390 cm^{-1} which are due to the physisorption of water molecule from the solution and absorbed OH^- from basic reagent for t_{MF}, 0 h and 24 h, respectively. Also, in the presence of EMF the peak at 1570 cm^{-1} is related to δH_2O.

3.3. Morphology, size, and size distribution

The TEM images of manganese oxides in neutral media under different conditions show the cubic and the rod-like structures (Supplementary Fig. S5). The TEM results confirm that the amount of nanorods is higher in the samples obtained with EMF especially under O_2 atmosphere. Figs. 2a, 3 a and 4a represent the HRTEM images of the samples in neutral medium with and without EMF. It reveals that the particle size can be varied with conditions. In neutral medium without EMF, smaller nanoparticles with an average size of 38 nm and a few amounts of nanorods with an average diameter of 25 nm and a length in the range of 200–400 nm were obtained. In neutral medium with EMF, a larger size of nanoparticles was obtained with an average diameter of 82 nm. Also, nanorods were obtained with an average diameter of 70 nm and the length in the range of 650–1300 nm (Fig. 3). By using O_2 atmosphere in neutral medium and in the presence of EMF, the average size of nanoparticles was about 60 nm and the nanorods were in an average diameter of 21 nm and a length in the range of 200–500 nm. The size distribution was obtained from the HRTEM and the monodisperse nanoparticles were achieved in the neutral medium without EMF. In the presence of EMF, less uniformity in size was obtained and the nanorods were existed in the form of bunches specially in the O_2 atmosphere due to agglomeration (Figs. 3a and 4a). According to these results, the size of nanoparticles and nanorods increased in the presence of EMF at longer times (t_{MF}, 24 h). The interplanar spacing was 2.8 Å, corresponding to (1 0 3) plane of Mn_3O_4 and 2.4 Å, corresponding to (2 1 1) plane of Mn_3O_4 for the nanoparticles obtained in the absence and presence of EMF, respectively (Figs. 2c and 3b). The selected-area electron diffraction pattern (SAED) of the nanoparticles are shown in Figs. 2e, 3c, and 4c. Actually, the nanocrystals are singlecrystalline in nature. But, the SAED patterns exhibit too many nanoparticles which led to polycrystalline pattern.

According to the TEM image, the size of nanoparticles is smaller in the basic condition than the neutral one (Supplementary Fig. S6). The samples in the basic medium consist mainly cubic nanoparticles with an average size of 14 nm, and 10 nm in the presence and absence of EMF. Some rod-like structure was also obtained in both conditions. In the absence of EMF, the diameter of rod-like was around 12 nm and the length was in the range of 100–900 nm. In the presence of EMF, the average diameter was obtained around 19 nm and the length was in the range of 900 nm to a few micrometers. In both cases, some of the nanoparticles were attached on the surface of the nanorods. There were not significant differences between the samples in the presence and absence of EMF in the basic condition. The HRTEM image, the corresponding SAED pattern, and the lattice image are shown in Fig. 5a–e. The HRTEM confirms the results obtained with XRD about the tetragonal phase of Mn_3O_4 and the observed lattice spacing of 2.6 Å and 2.9 Å correspond to the (1 0 3) and (1 1 2) planes of tetragonal Mn_3O_4, respectively. The chemical composition of the nanoparticles has been analyzed using EDS analysis (Supplementary Fig. S7). These nanoparticles obtained in the basic condition without EMF. The Cu peaks are the signal detected from the TEM grid. This result confirms the presence of Mn and O in the prepared samples. The EDS analysis of the other samples was found similar to that of the latter case (not shown).

3.4. Magnetic measurements

The hysteresis loops for the samples in neutral and basic media at 300 K are displayed in Fig. 6a, and b. All samples present a

Table 1
Type of manganese oxide nanoparticle according to the XRD pattern in different conditions.

Conditions	t_{MF} = 0 h	t_{MF} = 2 h	t_{MF} = 24 h
Bath	Mn_3O_4 (100%)	Mn_3O_4 (95%), MnO_2 (5%)	Mn_3O_4 (64.22%), MnOOH (24.7%), MnO_2 (6%), Mn_2O_3 (5%)
Bath-NaOH	Mn_3O_4 (100%)	Mn_3O_4 (86%), MnO_2 (5%), Mn_2O_3 (9%)	Mn_3O_4 (81.75%), MnO_2 (9%), Mn_2O_3 (9.5%)
Bath-O_2	Mn_3O_4 (100%)		Mn_3O_4 (85%), MnOOH (12%), Mn_2O_3 (3%)

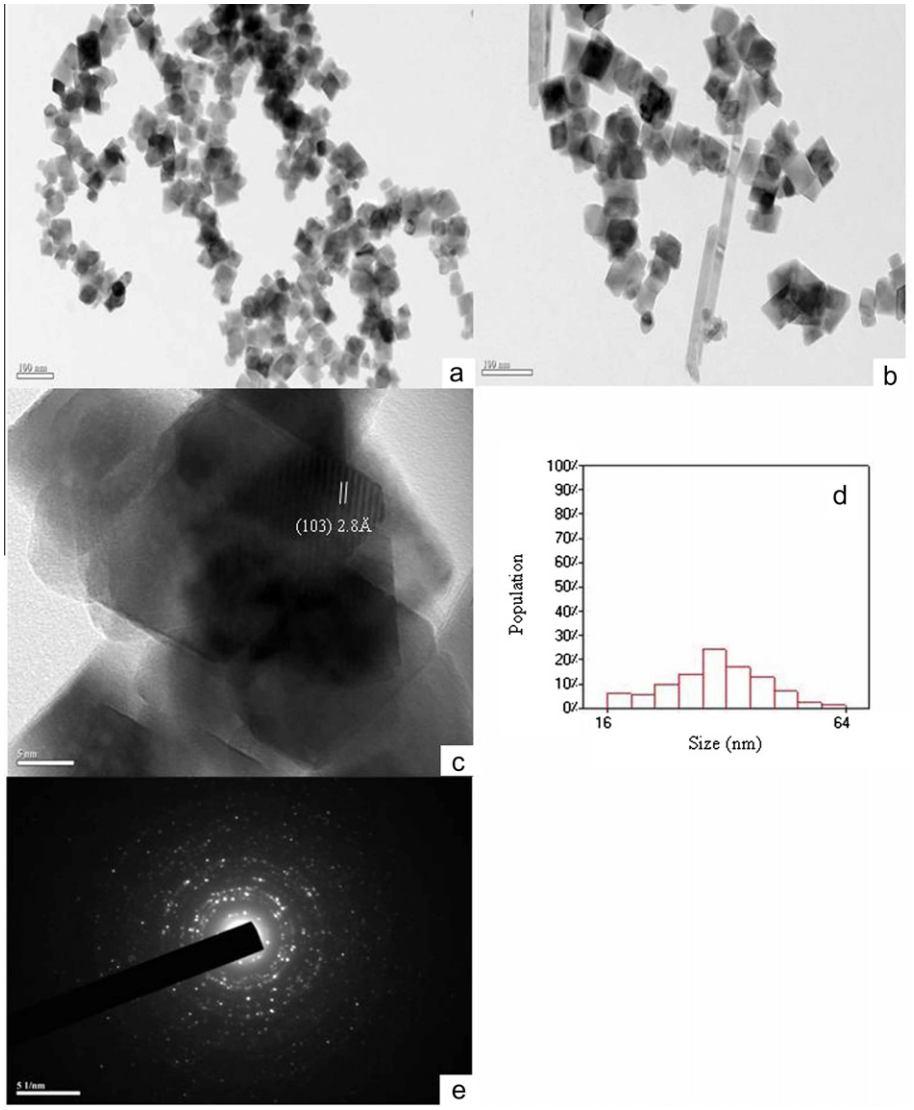

Fig. 2. (a, b) HRTEM, (c) lattice image, (d) histogram showing the particle size distribution measured from (a), and (e) SAED pattern of manganese oxide nanocrystal using ultrasonic irradiation in neutral medium without EMF (scale: a, b, 100 nm; c, 5 nm; e, 51 nm).

superparamagnetic behavior at room temperature. The magnetization versus field (*M–H*) is linear and no coercivity is observed. The hysteresis loop in the single domain is disappearing when the particle size becomes so small that the maximum anisotropy energy reaches to the thermal energy. Under this condition the ferro or ferrimagnetism called "superparamagnetism" as it does not show any hysteresis in *M–H* graph and the magnetization never get saturated even at very high applied field. It has also been reported that the nanorods can exhibit superparamagnetic behavior [45,46]. The reaction conditions can affect on the maximum magnetization at room temperature. The maximum values of magnetization are 3 emu/g, 2 emu/g, and 0.8 emu/g in the field of 20,000 Oe for the samples obtained in neutral medium with different time of magnetization (t_{MF}, 0 h, 2 h , and 24 h), respectively. In the field of 10,000 Oe, the amount of magnetization changes to 1.5 emu/g, 1.2 emu/g, and 0.3emu/g, respectively. It is indicated that the amount of magnetization decreased with increasing of t_{MF}. In the basic condition, the maximum value of magnetization was 0.5 emu/g in the field of 10,000 Oe for both samples, with (t_{MF}, 24 h) and without EMF. It means that in the basic medium, the presence or absence of EMF has no effect on the magnetization value. It is worth to mention that the loops are shifting in neutral medium and the amount of shift increases with the increase of t_{MF}. It is not well understood what cause gives rise to a shift of the hysteresis loop of the superparamagnetic nanomaterials along the field axis. It might be related to the presence of γ-MnOOH as an impurity phase in the sample. These observations about the magnetization of manganese oxide nanoparticles at room temperature are completely new.

A large coercivity and hysteresis loop are observed at temperature below T_c (10 K) for the sample prepared in basic medium with and without EMF (Fig. 7). The saturation magnetization (Ms) is not reached even at 10,000 Oe applied magnetic field. The maximum value for the magnetization at 10 K is about 28.4 emu/g and 30 emu/g for the samples in basic condition with t_{MF}, 0 h and 24 h, respectively. It is revealed that the EMF has no significant effect on the sample in basic condition. The coercivity fields are 3515 Oe for t_{MF}, 0 h and 4518 Oe for t_{MF}, 24 h which are larger than the value of 2800 Oe for the bulk samples under EMF. The obtained data exhibit smaller coercivity in comparison with the value reported by Qian and co-workers (6177 Oe) [45]. The smaller coercivity may be related to the mixture of nanorods and

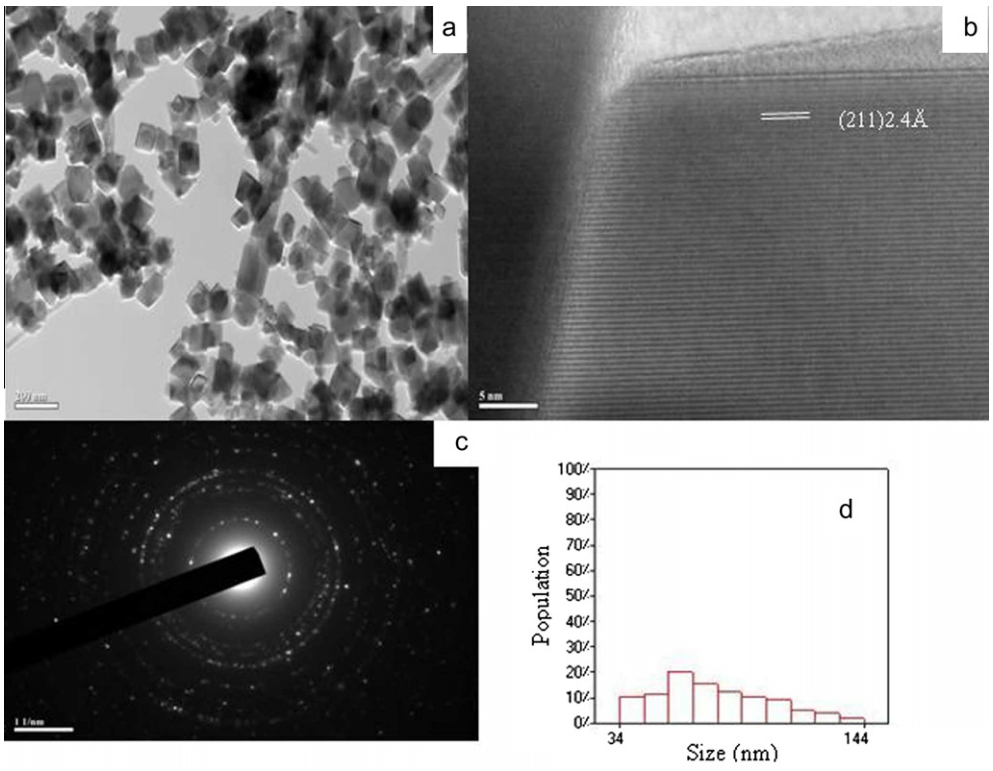

Fig. 3. (a) HRTEM, (b) lattice image, (c) SAED pattern , and (d) histogram showing the particle size distribution measured from (a) of manganese oxide nanocrystal using ultrasonic irradiation in neutral medium with EMF (t_{MF}, 24 h) (scale: a, 200 nm; b, 5 nm; c, 11 nm).

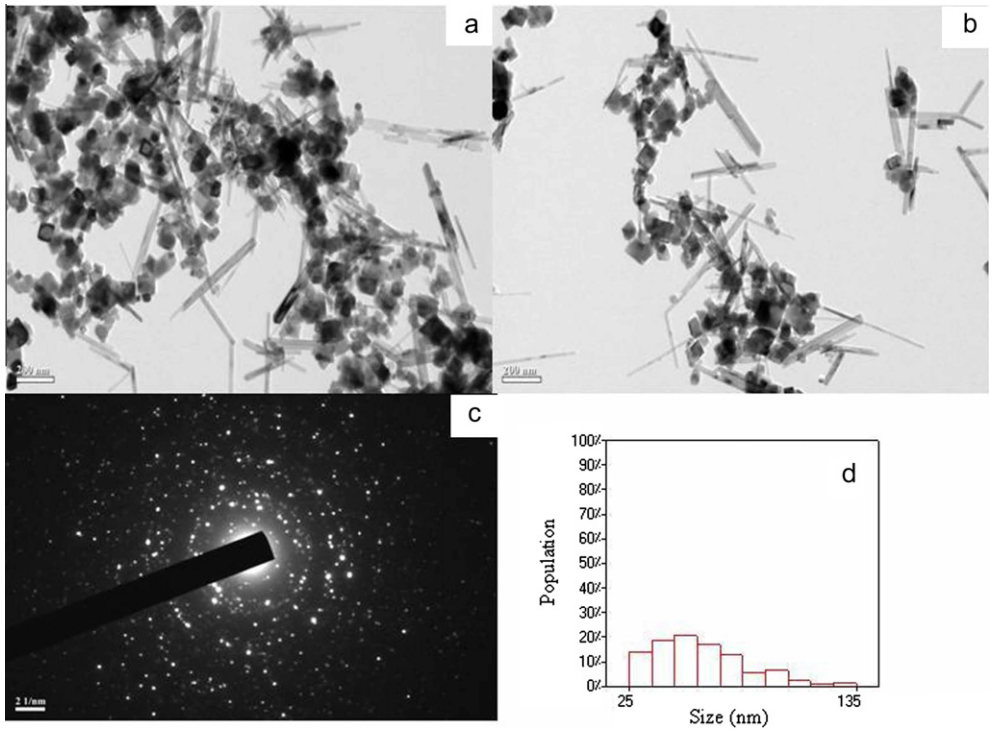

Fig. 4. (a, b) HRTEM, (c) SAED pattern, and (d) histogram showing the particle size distribution measured from (a) of manganese oxide nanocrystal using ultrasonic irradiation in neutral medium and O_2 atmosphere with EMF (t_{MF}, 24 h), (scale: a, b, 200 nm; c, 21 nm).

nanoparticles in the products. The observed large coercivity force in the products may also be related to the single-domain nature of the sample [47].

Magnetization as a function of temperature (M–T curves), FC (with field of 1000 Oe) and ZFC for the samples obtained in the basic condition at t_{MF}, 0 h and 24 h are shown in Figs. 8a and 9a. The

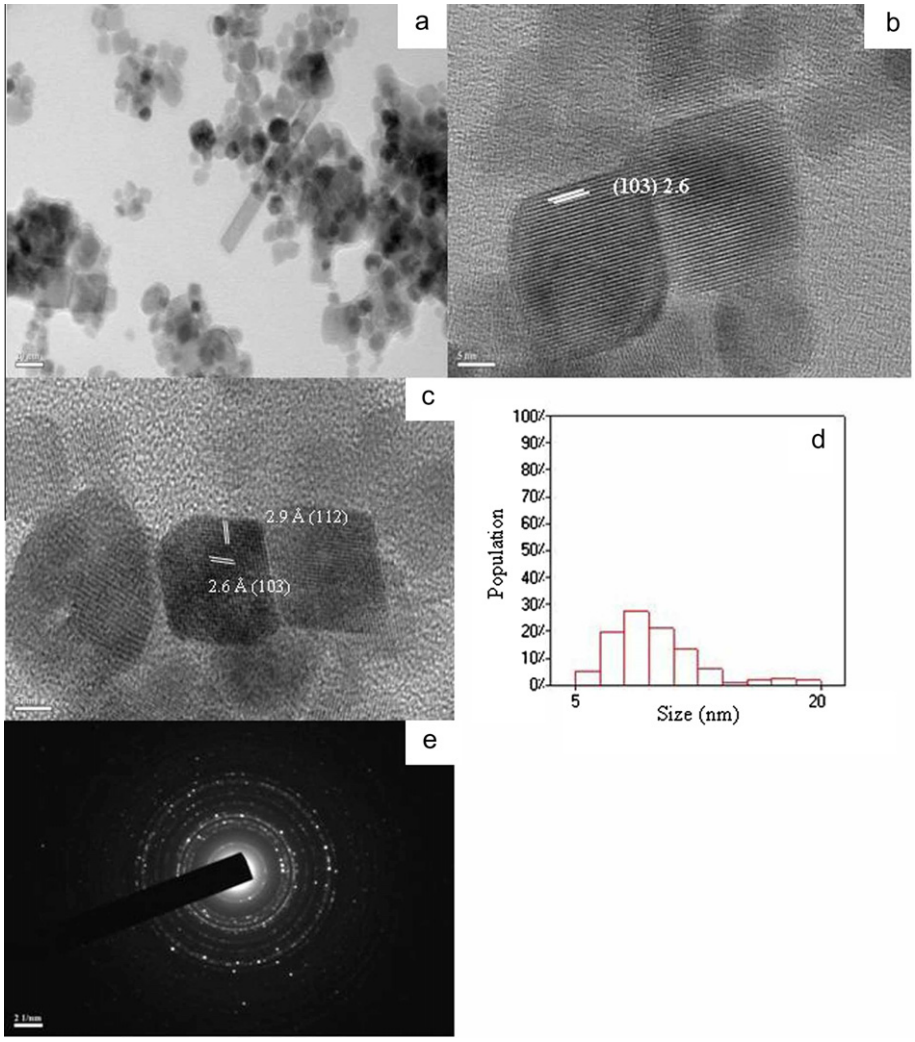

Fig. 5. (a) HRTEM, (b, c) lattice image, (d) histogram showing the particle size distribution measured from (a), and (e) SAED pattern of manganese oxide nanocrystal using ultrasonic irradiation in basic condition without EMF (scale: a, 20 nm; b, c, 5 nm; e, 21 nm).

magnetization decreases by increasing the temperature up to 39 K and then both samples sharply decrease around 44 K. The magnetization almost disappear in temperatures in the range of 44–295 K. The transition point in magnetic characteristics of the sample which is generally called T_c, can be determined more accurately by the derivative of magnetizations with respect to the temperature (Figs. 8b and 9b). The transition temperatures, T_c, are found at 40 K and 39 K for the samples in t_{MF}, 0 h and 24 h, respectively. These values are lower than that observed for the bulk Mn_3O_4 (43 K) [48,14]. In the present study, the observation of lower value of the ferrimagnetic onset temperature (T_c) in respect to the reported value for the bulk indicates that the particles are single domain in nature. Goplakrishnan et al. [24] presented the synthesis of nanocrytalline Mn_3O_4 by high intensity of ultrasonic irradiation and showed that the T_c was 39 K for nanoparticles with size of 15 nm. The bulk ferrimagnetic compound is multidomain in nature below its ferrimagnetic transition temperatures. The multidomain properties of a ferrimagnetic system can be lost if the particle size is decreased below a critical size. The sample exhibits an obvious ferrimagnetic behavior at low temperature.

3.5. Proposed mechanism

Manganese(II) salts aqueous solutions in the presence of strong bases form the pink-colored, insoluble manganese(II) hydroxide, $Mn(OH)_2$. In the presence of air and oxygen, $Mn(OH)_2$ is gradually oxidized to form dark-brown products which includes $Mn(OH)_3$ or probably MnO, and $MnO_2{\cdot}nH_2O$. Manganese(II) hydroxide is a fairly weak base and when heated in the presence of air, it produces Mn_3O_4 [49].

It is known that the sonochemical reaction does not happen inside the cavity which is due to the ionic structure of precursors (manganese acetate). Therefore, the reaction can facilitate at the interface of the bubble or in the bulk of the solution. A proposed mechanism for the formation of Mn_3O_4 under ultrasound from aqueous manganese acetate in air atmosphere is as follows:

$$H_2O \xrightarrow{)))))} H^{\cdot} + OH^{\cdot} \quad (1)$$

$$OH^{\cdot} + OH^{\cdot} \rightarrow H_2O_2 \quad (2)$$

In addition, according to Okitsu et al. [50], OOH radicals can be formed by the reaction of H radicals with O_2 molecules in air atmosphere and then the recombination of OOH radicals form H_2O_2:

$$H^{\cdot} + O_2 \rightarrow {\cdot}OOH \quad (3)$$

$$2{\cdot}OOH \rightarrow H_2O_2 + O_2 \quad (4)$$

The oxidant (H_2O_2) arises by ultrasound can initiate the oxidation of Mn^{2+}:

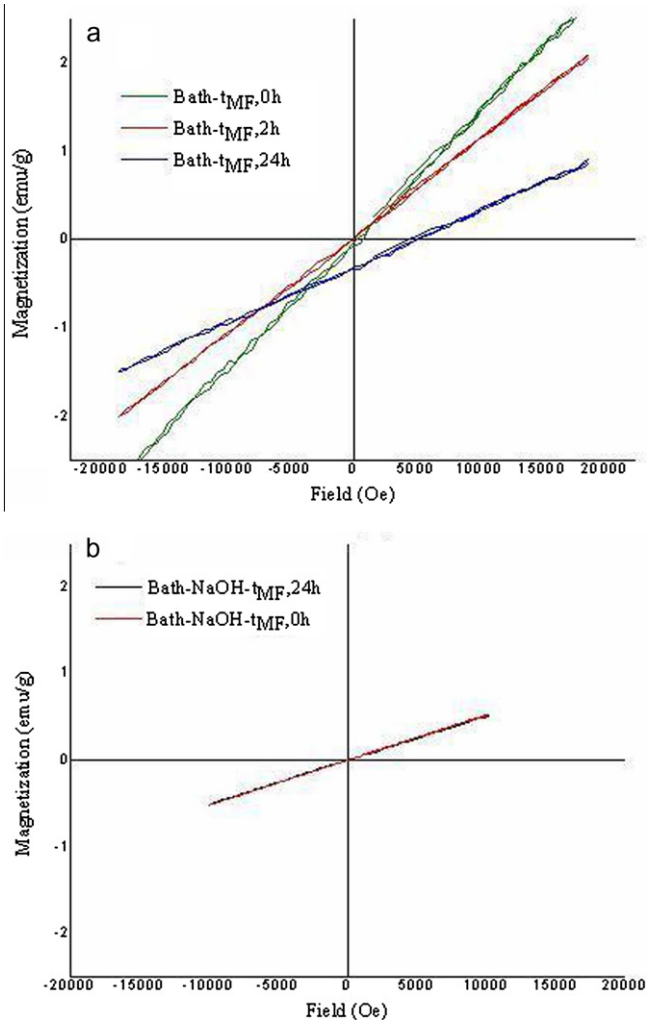

Fig. 6. Hysteresis loop of manganese oxide nanocrystal using ultrasonic irradiation in (a) neutral medium, and (b) basic condition with different t_{MF} at room temperature.

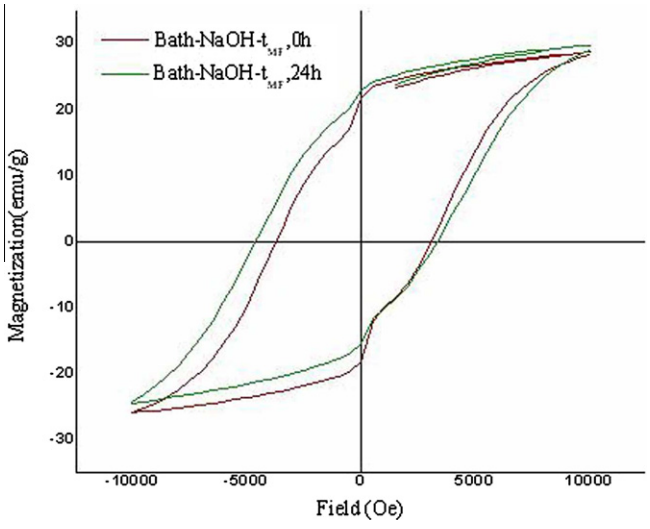

Fig. 7. Hysteresis loop of manganese oxide nanocrystal using ultrasonic irradiation in basic condition with different t_{MF} at 10 K.

$$3Mn(CH_3COO)_2 + 2H_2O + H_2O_2 \xrightarrow{)))))} Mn_3O_4 + 6CH_3COOH \quad (5)$$

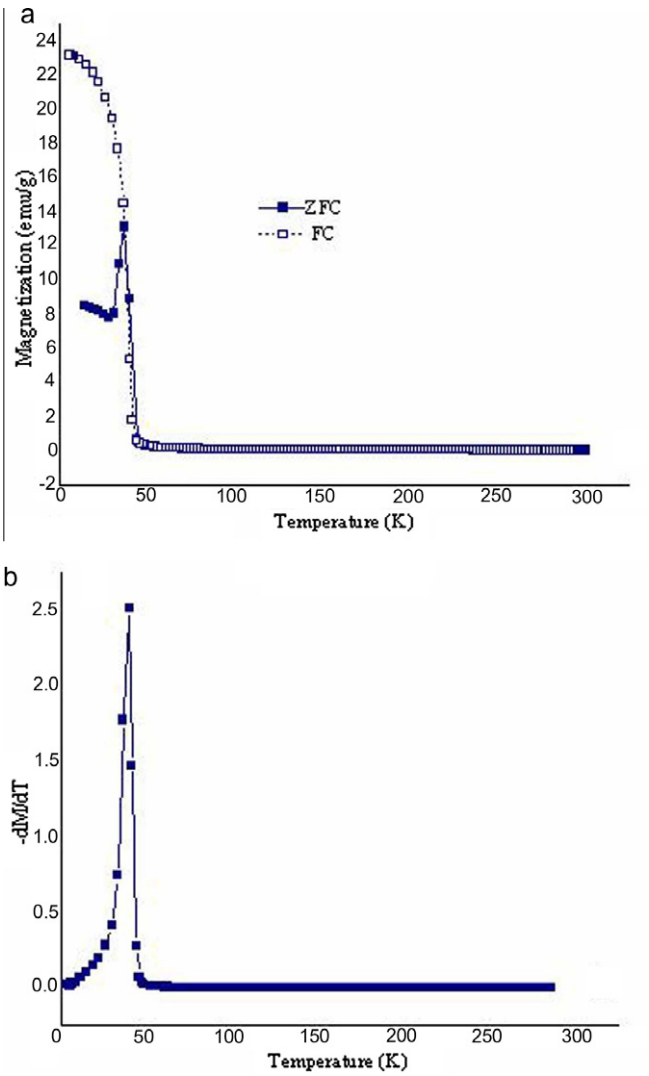

Fig. 8. (a) *M–T* curve of manganese oxide nanocrystal using ultrasonic irradiation in basic condition, (b) temperature derivative of magnetization vs. temperature (t_{MF}, 0 h).

As the amount of products was negligible in Ar atmosphere, Eq. (5) cannot be the main reaction. The results exhibited that air and O_2 have crucial role in neutral medium, therefore, the main reaction should be as follows:

$$3Mn(CH_3COO)_2 + 3H_2O + \frac{1}{2}O_2 \xrightarrow{)))))} Mn_3O_4 + 6CH_3COOH \quad (6)$$

In addition, in the basic solution, the following reactions can be occurred [51]:

$$6Mn^{2+} + 12OH^- + O_2 \rightarrow 2Mn_3O_4 + 6H_2O \quad (7)$$

The main finding of the experimental investigation in the presence and absence of EMF can be summarized as follows:

(1) The results show that the increase of EMF exposure time from 2 h to 24 h led to increase of induction period, increase of particle size, increase of nanorods, and decrease of magnetization in neutral medium.

(2) The magnetic field exposure was retarded the nucleation rate and accelerated the crystal growth. The same behaviors were observed by others [3,52]. The induction period in the presence of EMF was longer than its absence. The average size of nanoparticles in the presence and absence of EMF was 82 nm and 38 nm, respec-

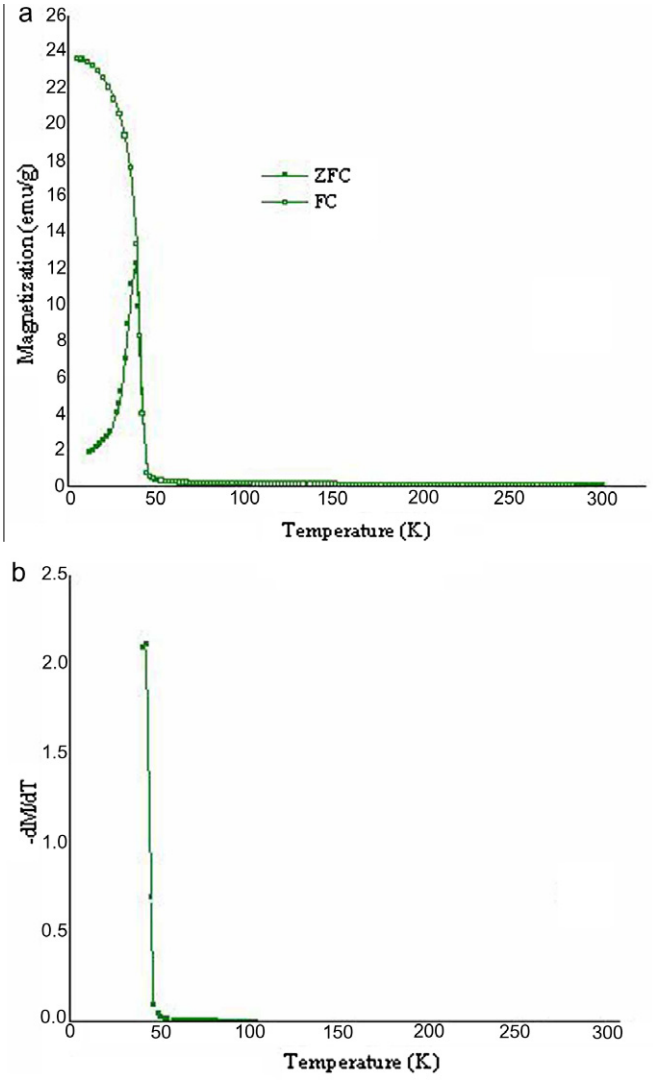

Fig. 9. (a) *M–T* curve of manganese oxide nanocrystal using ultrasonic irradiation in basic condition and (b) temperature derivative of magnetization vs. temperature (t_{MF}, 24 h).

tively. When oxygen atmosphere was used in the reaction media, the induction period was reduced which confirms the acceleration of nucleation rate. By increasing of O_2 concentration as precursor, the amount of nuclei was increased and led to decrease of the size (60 nm) in comparison with magnetic treatment without oxygen.

(3) The EMF can be led to an increase of dissolved oxygen concentration in the water from gas phase [53]. The obtained mixture of hausmannite and manganite in the presence of EMF might be related to the oxidation of Mn_3O_4 by oxygen (Eq. (8)) [42,54]:

$$\frac{1}{3}Mn_3O_4 + \frac{1}{12}O_2 + \frac{1}{2}H_2O \rightarrow MnOOH \quad (8)$$

Therefore, the γ-MnOOH phase can be synthesized with magnetic treatment of manganese acetate solution. In addition, in the presence of excess oxygen (O_2 atmosphere) as oxidizing agent, the following reactions were proposed:

$$4MnOOH + O_2 \rightarrow 4MnO_2 + 2H_2O \quad (9)$$

$$6MnO_2 \rightarrow 3Mn_2O_3 + \frac{3}{2}O_2 \quad (10)$$

$$3Mn_2O_3 \rightarrow 2Mn_3O_4 + \frac{1}{2}O_2 \quad (11)$$

For this reason, the amount of γ-MnOOH decreased by increasing of oxygen in the solution with respect to the sample obtained by magnetic treatment with t_{MF}, 24 h in ambient atmosphere.

(4) The EMF was promoted the formation of rod-like structure, especially in the presence of O_2 atmosphere. In diffusion-controlled growth process, the incoming flux toward each nanocrystal depends on the precursor concentration in the bulk solution. At high concentrations, the incoming precursors were diffused into the diffusion sphere and consumed mainly by the facet perpendicular to the axis which is more active than the other axis (easy-axis) of nanocrystals and resulted in a one-dimensional (1-D) growth stage [55,56]. The chemical potential of elongated nanocrystals should be high and it requires a relatively high potential medium which is achieved by a relatively high precursor concentration in the solution [55,56]. It is also known that, the high precursor concentration could be affected the formation of nuclei.

The Gibbs–Thampson equation is the basis of the classical crystallization theory [57]:

$$S_r = S_b \exp\left(\frac{2\sigma V_m}{rRT}\right) \quad (12)$$

where r is the radius of the crystal, σ is the specific surface energy, V_m is the molar volume of the substance, S_b and S_r are the solubility of bulk crystals and crystals with a radius r, R is the gas constant, and T is the absolute temperature. The Gibbs–Thompson equation describes that the solubility of a given crystal is strongly dependent on its size.

By changing Eq. (12) to Eq. (13):

$$RT \ln S_r = RT \ln S_b + \frac{2\sigma V_m}{r} \quad (13)$$

If μ_r and μ_b show the chemical potential of the crystals with a radius r and bulk, respectively, Eq. (13) can be converted to Eq. (14):

$$\mu_r = \mu_b + \frac{2\sigma V_m}{r} \quad (14)$$

For spherical crystals, the number of the surface atoms and the total atoms should be proportional to the surface area and the volume, respectively. If the surface atom ratio is defined as δ, then:

$$\delta = (k_1 4\pi r^2)/(k_2 4\pi r^3/3) = k_3 1/r \quad (15)$$

k_1, k_2, and k_3 are all proportional constants.

From Eqs. (14) and (15), the chemical potential of crystal proportional to their surface atom ratio and inversely proportional to the radium of the crystal:

$$\mu_r \propto \delta \propto \frac{1}{r} \quad (16)$$

Based on the Gibbs–Thompson equation, the minimum stable size of the nuclei (critical nuclei) which can be formed in the solution requires having a lower chemical potential than the precursors in the solution. Therefore, the higher amount of precursors led to smaller size of critical nuclei with higher surface area.

It is proposed that the continuous injection of oxygen as precursor during the reaction can be led to a high chemical potential of solution and formation of nanorods with faster growth in the long axis than the short axis during the reaction. In addition, the high chemical potential of solution can cause a decrease of induction period from 30 min to 10 min due to the rapid and easy nucleation of the process. The higher amount of dissolved oxygen in the presence of EMF can cause the higher amount of nanorods than its absence. It has suggested that for the diffusion-controlled crystal growth

each crystal is surrounded by a diffusion sphere [56]. It is assume that ultrasonic irradiation promotes the mass transfer and diffusion of precursors from the bulk into the diffusion sphere, so the facets along the axis which are more active should be quickly grow and led to the production of 1D structure. The other important parameter is the thickness of diffusion sphere which assume that ultrasonic irradiation can cause the decrease of thickness of diffusion sphere and increase of flux diffusion and faster growth along the active axis. In addition, under continuous sonication, the oriented attachment process is occurred by mechanism of alignment and coalescence between particles. In the basic medium, NaOH as a basic agent has a strong capping effect on the surface of nanoparticles and hinder the OR growth. Therefore, the size of nanoparticles cannot increase significantly and the size is nearly the same in the presence and absence of EMF.

(5) The results reveal that the process under Ar atmosphere led to a few amount of products and also no products were obtained in the absence of ultrasonic irradiation in neutral medium. These observations confirm the critical role of oxygen and ultrasonic irradiation to obtain the product in neutral medium.

4. Conclusion

Manganese oxide nanocrystals were synthesized via sonication of magnetized precursor solution in the neutral and basic media. Based on XRD results, a mixture of mainly Mn_3O_4 and MnOOH phases were obtained by using EMF in the neutral medium. But, sonication of unmagnetized solution led to pure Mn_3O_4. The rod-like structure was formed in the presence of ultrasonic irradiation and the amount of nanorods increased with magnetic treatment especially in the oxygen atmosphere. The magnetic treatment was also retarded the nucleation process and accelerated the crystal growth. In basic medium, a difference was observed on the composition of the products between magnetic treated and untreated solution. A superparamagnetic behavior was observed at room temperature without any saturation magnetization and hysteresis in the measured field strength. The effect of EMF on the sample prepared in the basic medium was negligible but, in the case of neutral medium, the EMF affected the slope of the magnetization curves.

Acknowledgments

We would like to thank Dr. Shizhang Qiao and Dr. Muxina Konarova (ARC Centre of Excellence for Functional Nanomaterials, Australian Institute for Bioengineering and Nanotechnology, The University of Queensland) for helpful assistance in the evaluation of magnetic properties, HRTEM analysis and Mrs. R. Pesyan from Central Research Laboratory of Ferdowsi University of Mashhad for TEM analysis.

Appendix A. Supplementary data

Supplementary data associated with this article can be found, in the online version, at doi:10.1016/j.ultsonch.2011.11.019.

References

[1] A.M.B. Freitas, F.J.G. Landgraf, M.M. Seckler, M. Giulietti, The influence of magnetic field on crystallization from solutions, in: Paper presented at the International Conference of Industrial Crystallization, England, September 1999 (Proceedings in CD-ROM).
[2] J. Nývlt, J. Kricková, Der einflub des magnetischen feldes auf die keimbildung in wäbrigen lösungen von magnesiumsulfat, Chem. Technol. 28 (1976) 548–550.
[3] K. Higashitani, A. Kage, S. Kalamura, K. Imai, S. Hatade, Effects of magnetic field on the formation of $CaCO_3$ particles, J. Colloid Interf. Sci. 156 (1993) 90–95.
[4] H.E. Lundager Madsen, Influence of magnetic field on the precipitation of some inorganic salts, J. Cryst. Growth 152 (1995) 94–100.
[5] M.M. Mitrovic, Growth rate dispersion of small $MnCl_2{\cdot}4H_2O$ crystals. II. Growth in magnetic field, J. Cryst. Growth 112 (1991) 171–182.
[6] Y.F. Shen, R.P. Zerger, R.N. Deguzman, S.I. Suib, L. Mccurdy, D.I. Potter, C.L. Oyoung, Manganese oxide octahedral molecular sieves: preparation, characterization, and applications, Science 260 (1993) 511–515.
[7] J.H. Wu, S.P. Ko, H.L. Liu, M.-H. Jung, J.H. Lee, J.-S. Ju, Y.K. Kim, Sub 5 nm Fe_3O_4 nanocrystals via coprecipitation method, Colloids Surf. A 313–314 (2008) 268–272.
[8] D.C. Niu, Y.S. Li, Z. Ma, H. Diao, J.L. Gu, H.R. Chen, W.R. Zhao, M.L. Ruan, Y.L. Zhang, J.L. Shi, Preparation of uniform water-soluble and multifunctional nanocomposites with tunable sizes, Adv. Funct. Mater. 20 (2010) 73–780.
[9] W.D. Zhang, H.M. Xiao, L.P. Zhu, S.Y. Fu, Template-free solvothermal synthesis and magnetic properties of novel single-crystalline magnetite nanoplates, J. Alloys Compd. 477 (2009) 736–738.
[10] D. Amara, I. Felner, I. Nowik, S. Margel, Synthesis and characterization of Fe and Fe_3O_4 nanoparticles by thermal decomposition of triiron dodecacarbonyl, Colloids Surf. A 339 (2009) 106–110.
[11] D.R. Merrill, C.C. Scalion, The catalytic oxidation of carbon monoxide, J. Am. Chem. Soc. 43 (1921) 1973–1982.
[12] B. Nowack, A.T. Stone, Manganese-catalyzed degradation of phosphonic acids, Environ. Chem. Lett. 1 (2003) 24–31.
[13] Y.C. Zhang, T. Qiao, X.Y. Hu, Preparation of Mn_3O_4 nanocrystallites by low-temperature solvothermal treatment of γ-MnOOH nanowires, J. Solid State Chem. 177 (2004) 4093–4097.
[14] Y.Q. Chang, X.Y. Xu, X.H. Luo, C.P. Chen, D.P. Yu, Synthesis and characterization of Mn_3O_4 nanoparticles, J. Cryst. Growth 264 (2004) 232–236.
[15] S. Ching, J.L. Roark, N. Duan, S.L. Suib, Sol–Gel route to the tunneled manganese oxide cryptomelane, Chem. Mater. 9 (1997) 750–754.
[16] T. Ozkaya, A. Baykal, H. Kavas, Y. Koseoglu, M.S. Toprak, A novel synthetic route to Mn_3O_4 nanoparticles and their magnetic evaluation, Physica B 403 (2008) 3760–3764.
[17] H. Liu, H. Cui, F. Han, X. Li, J. Wang, R.I. Boughton, Growth of Bi_2Se_3 nanobelts synthesized through a co-reduction method under ultrasonic irradiation at room temperature, Cryst. Growth Des. 5 (2005) 1711–1714.
[18] S.-M. Zhou, X.-H. Zhang, X.-M. Meng, X. Fan, S.-T. Lee, S.-K. Wu, Sonochemical synthesis of mass single-crystal PbS nanobelts, J. Solid State Chem. 178 (2005) 399–403.
[19] M. Sivakumar, A. Towata, K. Yasui, T. Tuziuti, Y. Iida, A new ultrasonic cavitation approach for the synthesis of zinc ferrite nanocrystals, Curr. Appl. Phys. 6 (2006) 591–593.
[20] R.A. Caruso, M. Ashokkumar, Sonochemical formation of colloidal platinum, Colloids Surf. A 169 (2000) 219–225.
[21] A. Pradhan, R.C. Jones, D. Caruntu, C.J. O'Connor, M.A. Tarr, Gold–magnetite nanocomposite materials formed via sonochemical methods, Ultrason. Sonochem. 15 (2008) 891–897.
[22] V. Kesavan, P.S. Sivanand, S. Chandrasekaran, Y. Koltypin, A. Gedanken, Catalytic aerobic oxidation of cycloalkanes with nanostructured amorphous metals and alloys, Angew. Chem. Int. Ed. 38 (1999) 3521–3523.
[23] J.H. Bang, K.S. Suslick, Applications of ultrasound to the synthesis of nanostructured materials, Adv. Mater. 22 (2010) 1–21.
[24] I.K. Goplakrishnan, N. Bagkar, R. Ganguly, S.K. Kulshreshtha, Synthesis of superparamagnatic Mn_3O_4 nanocrystallites by ultrasonic irradiation, J. Cryst. Growth 280 (2005) 436–441.
[25] T. Rohani Bastami, M.H. Entezari, Sono-synthesis of Mn_3O_4 nanoparticles in different media without additives, Chem. Eng. J. 164 (2010) 261–266.
[26] V.G. Kumar, D. Aurbuch, A. Gedanken, A comparison between hot-hydrolysis and sonolysis of various Mn(II) salts, Ultrason. Sonochem. 10 (2003) 17–23.
[27] T. Rohani Bastami, M.H. Entezari, A novel approach for the synthesis of superparamagnetic Mn_3O_4 nanocrystals by ultrasonic bath, Ultrason. Sonochem., 2011, accepted for publication.
[28] X. Duan, Y. Huang, Y. Cui, J. Wang, C.M. Lieber, Indium phosphide nanowires as building blocks for nanoscale electronic and optoelectronic devices, Nature 409 (2001) 66–69.
[29] M.S. Gudiksen, U.J. Lauhon, J. Wang, D.C. Smith, C.M. Lieber, Growth of nanowire superlattice structures for nanoscale photonics and electronics, Nature 415 (2002) 617–620.
[30] D. Zhang, X. Zhang, X. Ni, J. Song, H. Zheng, Low-temperature fabrication of $MnFe_2O_4$ octahedrons: magnetic and electrochemical properties, Chem. Phys. Lett. 426 (2006) 120–123.
[31] J. Lao, J. Huang, D. Wang, Z. Ren, Self-assembled In_2O_3 nanocrystal chains and nanowire networks, Adv. Mater. 16 (2004) 65–69.
[32] Y. Li, M. Sui, Y. Ding, G. Zhang, J. Zhuang, C. Wang, Preparation of $Mg(OH)_2$ nanorods, Adv. Mater. 12 (2000) 818–821.
[33] Y.-W. Jun, M.F. Casula, J.-H. Sim, S.Y. Kim, J. Cheon, A.P. Aliyisatos, Surfactant-assisted elimination of a high energy facet as a means of controlling the shapes of TiO_2 nanocrystals, J. Am. Chem. Soc. 125 (2003) 15981–15985.
[34] B. Li, Y. Zhao, X. Xu, H. Zhou, B. He, Z. Wu, Z. Zhang, A simple method for the preparation of containing Sb nano- and microcrystallines via an ultrasound agitation, Ultrason. Sonochem. 13 (2007) 557–562.
[35] H. Li, H. Li, Z. Guo, Y. Liu, The application of power ultrasound to reaction crystallization, Ultrason. Sonochem. 13 (2006) 359–363.
[36] N. Amara, B. Ratsimba, A. Wilhelm, H. Delmas, Growth rate of potash alum crystals: comparison of silent and ultrasonic conditions, Ultrason. Sonochem. 11 (2004) 17–21.
[37] L.A. Crum, T.J. Mason, J.L. Reisse, K.S. Suslick, Sonochemistry and Sonoluminesence, Kluwer Academic Publishers, Washington, USA, p. 248.
[38] T.J. Mason, Sonochemistry, Oxford University Press, New York, 1999.

[39] S. Vajnhandi, A.M. Le Marechal, Case study of the sonochemical decolouration of textile azo dye reactive blue 5, J. Hazard. Mater. 141 (2007) 329–335.
[40] C.M. Julien, M. Massot, C. Poinsignon, Lattice vibrations of manganese oxides: Part I: Periodic structures, Spectrochim. Acta Part A 60 (2004) 689–700.
[41] T. Kohler, T. Armbruster, E.J. Libowitzky, Hydrogen bonding and Jahn–Teller distortion in Groutite, α-MnOOH, and manganite, γ-MnOOH, and their relations to the manganese dioxides ramsdellite and pyrolusite, J. Solid State Chem. 133 (1997) 486–500.
[42] S.A. Kirillov, V.S. Aleksandrova, T.V. Lisnycha, D.I. Dzanashvili, S.A. Khainakov, J.R. Garca, N.M. Visloguzova, O.I. Pendelyuk, Oxidation of synthetic hausmannite (Mn_3O_4) to manganite (MnOOH), J. Mol. Struct. 928 (2009) 89–94.
[43] A. Novak, Hydrogen bonding in solids correlation of spectroscopic and crystallographic data, Struct. Bond. 18 (1974) 177–216.
[44] M. Ishii, M. Nakahira, Infrared absorption spectra cation distributions in $(MnFe)_3O_4$, Solid State Commun. 11 (1972) 209–212.
[45] J. Du, Y. Gao, L. Chai, G. Zou, Y. Li, Y. Qian, Hausmannite Mn_3O_4 nanorods: synthesis, characterization and magnetic properties, Nanotechnology 17 (2006) 4923–4928.
[46] L. Sicard, J.-M. Le Meins, C. Methivier, F. Herbst, S. Ammar, Polyol synthesis and magnetic study of Mn_3O_4 nanocrystals of tunable size, J. Magn. Magn. Mater. 322 (2010) 2634–2640.
[47] T.M. Whiteny, J.S. Jiang, P.C. Searson, C.L. Chine, Fabrication and magnetic properties of arrays of metallic nanowires, Science 261 (1993) 1316–1319.
[48] G. Srinivasan, M.S. Seehra, Nature of magnetic transitions in MnO, Fe_2O, CoO, and NiO, Phys. Rev. B 28 (1983) 6542–6544.
[49] S.B. Parker, McGraw-Hill Encyclopedia of Chemistry. McGraw Hill, New York, 1993.
[50] K. Okitsu, K. Iwasaki, Y. Yobiko, H. Bandow, R. Nishimura, Y. Maeda, Sonochemical degradation of azo dyes in aqueous solution: a new heterogeneous kinetics model taking into account the local concentration of OH radicals and azo dyes, Ultrason. Sonochem. 12 (2005) 255–262.
[51] L.-X. Yang, Y. Liang, H. Chen, Y.-F. Meng, W. Jiang, Mn_3O_4 nanoplates and nanoparticles: synthesis, characterization, electrochemical and catalytic properties, J. Solid State Chem. 183 (2010) 744–751.
[52] R.A. Barrett, S.A. Parsons, The influence of magnetic field on calcium carbonate precipitation, Water Res. 32 (1998) 609–612.
[53] K. Kitazawa, Y. Ikezoe, H. Uetake, N. Hirota, Magnetic field effects on water, air and powders, Physica B 294–295 (2001) 709–714.
[54] R. Giovanoli, U. Leuenberger, Helv. Über die Oxydation von Manganoxidhydroxid, Chim. Acta 52 (1969) 2333–2347.
[55] Z.A. Peng, X. Peng, Nearly monodisperse and shape-controlled CdSe nanocrystals via alternative routes: nucleation and growth, J. Am. Chem. Soc. 124 (2002) 3343–3353.
[56] Z.A. Peng, X. Peng, Mechanisms of the shape evolution of CdSe nanocrystals, J. Am. Chem. Soc. 123 (2001) 1389–1395.
[57] J.W. Mullin, Crystallization, third ed., Butterworth - Heinemann Oxford, 1997.